action were performed with a contemporary stellar evolution code, which contains the most recent physics input (*22*). In particular, use of this code can produce up-to-date solar models (*23*) and can allow one to follow the evolution of low-mass stars through the thermal pulses of asymptotic giant branch (AGB) stars (*24*). The nuclear network is designed preferentially to calculate the H- and He-burning phases in low-mass stars. Additionally, the basic reactions of C- and O-burning are included, which may destroy the produced C and O in massive and intermediate-mass stars.

We performed stellar model calculations for a typical massive, intermediate-mass, and low-mass star with masses 20, 5, and $1.3M_{\odot}$, respectively. The stars are followed from the onset of H-burning until the third thermal pulse in the AGB, or until the core temperature reaches 10^9 K in the case of the $20M_{\odot}$ star (the nuclear network is not sufficient to go beyond this phase). For the $1.3M_{\odot}$ star, which loses its envelope by stellar winds during the thermal-pulse phase, the maximum C and O abundances in the He-burning region have been extracted. By taking the maximum abundances in this region, we have a measure of how much the envelope of the star can be enriched by C or O, irrespective of how efficient the dredge-up of heavy elements is compared with our model.

For the three stellar masses, the evolution is calculated with different values of the resonance energy in the triple-alpha reaction within a range to cover variations in the strength of the strong and Coulomb interaction up to 0.5 and 4%, respectively. The resulting modifications in the C and O abundances are shown (Fig. 1) with respect to the case, where the standard value of the resonance energy has been used (i.e., with no variations of the strength of the strong or Coulomb interaction). Because each shift in the resonance energy can be identified with a variation in the strength of the N-N or Coulomb interaction, we scaled the upper and lower ordinate with variations in these quantities. Our calculations indicate that the behavior of the residual alpha-alpha interaction, and thus that of the resonance energy of the 0_2^+ state, is expected to lie somewhere between the predictions of two of our effective N-N interactions, the MN (*10*, *11*) and the MHN (*12*) forces. Therefore, we show the abundances calculated only with these two effective N-N interactions (Fig. 1).

A saturation of the C production is reached with increasing N-N interaction (very pronounced for the $5M_{\odot}$ star) because no alpha particles are available below the He-burning front. Thus, the star does not gain additional energy from the $^{12}C(\alpha,\gamma)^{16}O$ reaction. The stellar core contracts more rapidly and C-destroying $^{12}C + {}^{12}C$ reactions ignite earlier. For O, a similar behavior can be observed with decreasing N-N interaction strength. Because the temperatures where the triple-alpha reactions set in are enhanced with decreasing N-N force, the temperatures below the He-burning shell are much higher than in the standard case, and $^{16}O + \alpha$ reactions can destroy the previously generated O more efficiently than in the standard case (0%).

We conclude that a change of more than 0.5% in the strength of the strong interaction or more than 4% change in the strength of the Coulomb force would destroy either nearly all C or all O in every star. This implies that irrespective of stellar evolution the contribution of each star to the abundance of C or O in the ISM would be negligible. Therefore, for the above cases the creation of carbon-based life in our universe would be strongly disfavored. The anthropically allowed strengths of the strong and electromagnetic forces also constrain the Higgs vacuum expectation value (*25*) and yield tighter constraint on the quark masses than do the constraints from light nuclei (*26*). Therefore, the results of this work are relevant not only for the anthropic cosmological principle (*27*), but also for the mathematical design of fundamental elementary particle theories.

References and Notes

1. D. N. F. Dunbar, R. E. Pixley, W. A. Wenzel, W. Whaling, *Phys. Rev.* **92**, 649 (1953).
2. F. Hoyle, D. N. F. Dunbar, W. A. Wenzel, *Phys. Rev.* **92**, 1095 (1953).
3. C. W. Cook, W. A. Fowler, T. Lauritsen, *Phys. Rev.* **107**, 508 (1957).
4. V. S. Shirley, Ed., *Table of Isotopes, Volume I* (Wiley, New York, ed. 8, 1996).
5. C. E. Rolfs and W. S. Rodney, *Cauldrons in the Cosmos* (Univ. of Chicago Press, Chicago, 1988).
6. M. Livio, D. Hollowell, A. Weiss, J. W. Truran, *Nature* **340**, 281 (1989).
7. H. Oberhummer, A. Csótó, H. Schlattl. Print available at http://xxx.lanl.gov/abs/astro-ph/9908247.
8. R. Pichler, H. Oberhummer, A. Csótó, S. A. Moszkowski, *Nucl. Phys. A* **618**, 55 (1997).
9. A. B. Volkov, *Nucl. Phys.* **74**, 33 (1965).
10. I. Reichstein and Y. C. Tang, *Nucl. Phys. A* **158**, 529 (1970).
11. D. R. Thompson, M. LeMere, Y. C. Tang, *Nucl. Phys. A* **286**, 53 (1977).
12. H. Furutani *et al.*, *Prog. Theor. Phys. Suppl.* **68**, 193 (1980).
13. R. Kippenhahn and A. Weigert, *Stellar Structure and Evolution* (Springer-Verlag, Berlin, 1990).
14. M. Schwarzschild and A. R. Härm, *Astrophys. J.* **142**, 855 (1965).
15. I. Iben and A. Renzini, *Ann. Rev. Astron. Astrophys.* **21**, 271 (1983).
16. A. Weiss, P. A. Denissenkov, C. Charbonnel, *Astron. Astrophys.* **356**, 181 (2000).
17. S. E. Woosley and T. A. Weaver, *Astrophys. J. Suppl. Ser.* **101**, 181 (1995).
18. K. Nomoto *et al.*, *Nucl. Phys. A* **616**, 79 (1997).
19. A. Maeder, *Astron. Astrophys.* **264**, 105 (1992).
20. F. X. Timmes, S. E. Woosley, T. A. Weaver, *Astrophys. J. Suppl. Ser.* **98**, 617 (1995).
21. R. B. C. Henry, K. B. Kwitter, J. A. Bates, *Astrophys. J.*, in press (e-print available at http://xxx.lanl.gov/abs/astro-ph/9910347).
22. A. Weiss and H. Schlattl, *Astron. Astrophys. Suppl.*, **144**, 487 (2000) (e-print available at http://xxx.lanl.gov/abs/astro-ph/9912310).
23. H. Schlattl and A. Weiss, *Astron. Astrophys.* **347**, 272 (1999).
24. J. Wagenhuber and A. Weiss, *Astron. Astrophys.* **286**, 121 (1994).
25. E. T. Jeltema and M. Sher, *Phys. Rev. D* **61**, 017301 (2000).
26. C. J. Hogan, e-print available at http://xxx.lanl.gov/abs/astro-ph/9909295.
27. J. D. Barrow and F. J. Tipler, *The Anthropic Cosmological Principle* (Oxford Univ. Press, Oxford, 1986).

28. Supported in part by the Fonds zur Wissenschaftlichen Forschung in Österreich (P10361-PHY), the OTKA Fund (D32513), the Education Ministry (FKFP-0242/2000), the Academy (BO/00520/98) in Hungary, and by the John Templeton Foundation (938-COS153).

14 March 2000; accepted 17 May 2000

Topographic Mapping of the Quantum Hall Liquid Using a Few-Electron Bubble

G. Finkelstein,[1] P. I. Glicofridis,[1] R. C. Ashoori,[1] M. Shayegan[2]

A scanning probe technique was used to obtain a high-resolution map of the random electrostatic potential inside the quantum Hall liquid. A sharp metal tip, scanned above a semiconductor surface, sensed charges in an embedded two-dimensional (2D) electron gas. Under quantum Hall effect conditions, applying a positive voltage to the tip locally enhanced the 2D electron density and created a "bubble" of electrons in an otherwise unoccupied Landau level. As the tip scanned along the sample surface, the bubble followed underneath. The tip sensed the motions of single electrons entering or leaving the bubble in response to changes in the local 2D electrostatic potential.

Since the discovery of the integer quantum Hall effect (QHE) in a two-dimensional electron gas (2DEG), electron localization has been proposed to play a key role in the phenomenon (*1*). In GaAs heterostructures, the random potential responsible for localization derives mainly from randomly situated ionized donors, located between the submerged 2DEG and the sample surface. Although this picture remains widely used, it has proven difficult to quantify the random potential experimentally. Conductivity measurements, the

primary tool for studying the QHE, provide only average information about the disorder. Recently developed scanning techniques hold promise for spatially resolving the behavior of semiconductor structures on nanometer scales (*2*–*6*). In particular, low-compressibility strips (*7*) with Landau level–filling factor ν close to an integer have been imaged directly in the integer quantum Hall regime (*5, 6*).

We present results from a new technique that images microscopic details of the disorder potential through the detection of motions of single electrons within the system under study. A mobile quantum dot is created inside the 2DEG by enhancing the 2DEG density locally underneath a sharp scanned metal tip biased to attract electrons. While scanning the tip across the sample surface, we drag the dot along underneath. Comparing the single-electron charging pattern of the dot at different locations, we map the electrostatic potential directly as sensed by the 2DEG electrons. We find that the form of this potential remains mostly unchanged for different spin-split and integer Landau level fillings, which suggests that screening of the random external potential by the 2D electrons does not vary appreciably in the quantum Hall regime.

Our 2DEG is formed at the GaAs-AlGaAs interface 80 nm below the sample surface, and it has an electron density of $\sim 1.5 \times 10^{11}$ cm^{-2} and mobility of $\sim 1.5 \times 10^{6}$ cm^2 V^{-1} s^{-1}. A metallic gate electrode, patterned in the form of a grating, covers the sample surface (Fig. 1). We image a region of the surface several micrometers in size between two fingers of the gate. In the subsurface charge accumulation (SCA) method (*3, 6*), a sharp scanning probe is brought close ($\leq$20 nm) to the surface of the sample. Unlike scanning tunneling microscopy, no tunneling current passes between the probe and the sample. Instead, we apply a 100-kHz ac excitation of $\sim$3 mV (root mean square) to the 2DEG and to the gate. Because of the capacitance of the 2DEG to the ground and to the scanning tip, electric charge flows in and out of the 2DEG. We monitor this charging of the 2DEG by measuring the image charge induced on the scanning probe by a sensitive cryogenic amplifier.

In scanning probe measurements of semiconductor and nanoscale structures, the measuring tip may itself strongly alter the local electron density and thus produce artifacts in images. Some researchers have taken advantage of this effect by using a scanning tip to alter the current flow in nanoscale systems (*2*). In previous work using SCA microscopy, we compensated the work function difference between the scanning tip and the sample to avoid the tip perturbing the sample electrostatically (*3, 6*). The resulting SCA images revealed features attributed to variations of the 2DEG compressibility. In the present work, we instead purposefully apply a voltage on the scanning tip to change the electron density underneath. For magnetic fields such that the bulk Landau level–filling factor is slightly less than integer, we thereby create a "bubble" of electrons in the next Landau level (inset, Fig. 2). The electrons in the bubble are separated from the surrounding 2DEG by an incompressible strip (*7*) of integer Landau level filling. The imaged features do not display the compressibility variations inherent in the 2DEG. Instead, Coulomb blockade in the bubble determines the observed signal, and the images display a set of equipotential contours that serve as a topographic map of the random electrostatic potential in the 2DEG. One may "read" directly the electrostatic potential by noting the positions of the contours.

We find the voltage that compensates the electric field between the tip and the sample by measuring the Kelvin signal (see Fig. 1) (*8*), which is proportional to the electrostatic potential difference between the tip and the sample. With no external bias applied between them, the electrostatic potential difference equals the work function difference between the two. We null it by applying an opposing bias to eliminate any electric field between the tip and the sample. Henceforth, we designate the tip-sample voltage as measured in deviation from this nulling voltage.

In the SCA image of a 2.5 μm by 2.5 μm region at magnetic fields of 5.8 T, corresponding to the bulk Landau level–filling factor $\nu = 1$ (Fig. 2A), regions of high and low signal are presented as bright and dark colors, respectively. The voltage between the tip and the sample is +1 V. This corresponds to accumulation of the electrons underneath the tip. We observe a strikingly complex pattern of closed contours, reminiscent of a topographic map. The contours evolve rapidly with increasing magnetic field, staying nested around fixed centers.

The size of the smallest feature within 2DEG resolvable by the SCA microscopy is limited by the depth of the 2DEG, $d = 80$ nm. However, we measure separations between contour lines as small as 50 nm. Therefore, we conclude that the contours do not represent charging patterns inherent in the 2DEG. Rather, the features reflect variations in the 2DEG charging induced by changes of the tip position. The periodic appearance of the contours hints that they originate from Coulomb blockade (*9*). Indeed, when we fix the tip position and vary the tip-sample voltage, the signal displays periodic oscillations. In this situation, the tip acts as a gate controlling the electron number in a quantum dot (*9*).

We explain the observed contours as follows. An electron accumulation underneath the tip forms a few-electron bubble (inset, Fig. 2). As the bubble is dragged in the 2DEG plane following the tip, it experiences different local electrostatic potentials. When the potential energy for electrons is high, electrons are expelled from the bubble; when the potential energy is low, electrons are drawn into the bubble. As the tip scans across these positions of single electron transfer, the applied ac excitation causes an electron to move back and forth between the bubble and the surrounding 2DEG, producing a peak in the synchronously detected SCA signal (*10*). Between the peaks, Coulomb blockade prohibits transfer of electrons to and from the bubble, and a minimum of SCA signal is detected. As a result, SCA images display alternating con-

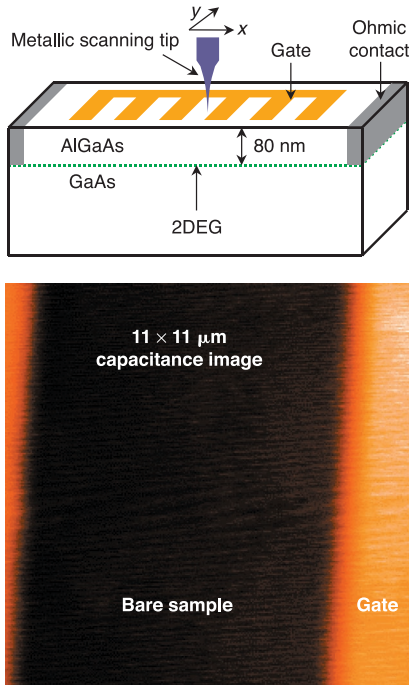

Fig. 1. Sample and measurement schematics. Upper panel: The charge accumulation (capacitance) method with an ac excitation applied to the sample and the gate. Capacitive coupling between the tip and the 2DEG induces an ac signal on the tip. Lower panel: Capacitance image of an 11 μm by 11 μm region, including two "fingers" of the gate. The gate resides directly on the surface of the semiconductor, whereas the 2DEG is buried underneath the surface. Therefore, the gate produces a larger capacitance signal. In the Kelvin probe method, we vibrate the sample in the vertical direction with a frequency of 2 kHz and an amplitude of $\sim$10 nm. We measure the ac charge induced on the scanning probe. It is proportional to $V\, dC/dz$, where C is the probe-sample capacitance, z is the tip height, and V is the electrostatic potential difference between the tip and the sample.

[1]Department of Physics and Center for Materials Science and Engineering, Massachusetts Institute of Technology, Cambridge, MA 02139, USA. [2]Department of Electrical Engineering, Princeton University, Princeton, NJ 08544, USA.

tours of high and low SCA signal surrounding minima and maxima of the random electrostatic potential within the 2DEG.

The contours observed in the experiment do not intersect, and they have roughly the same contrast across the image. This confirms that they originate from a single bubble located underneath the tip (*11*). The fact that contours appear only on the high magnetic field side of the quantum Hall plateau also supports this scenario. Four images at different magnetic fields around $\nu = 1$ are shown in Fig. 2C. For the top three images, the Landau level–filling factor in the bulk of the sample is $\nu < 1$, while underneath the tip it is $\nu > 1$. The bubble of $\nu > 1$ is separated from the bulk by the incompressible strip with $\nu = 1$ (inset, Fig. 2). The strip serves as a barrier between the bulk 2DEG and the bubble and ensures charge quantization (*12*). In contrast, at the lower field side of the quantum Hall plateau (lowest image, Fig. 2C), the filling factor is everywhere larger than 1 and a mere density enhancement forms, rather than a bubble capable of trapping single electrons.

We show the evolution of SCA images at 6 T with different tip-sample voltages in Fig. 2D. As the voltage decreases (lower images), the contours shrink and disappear around nulling voltage (*13*). Without electric field between the tip and the sample, the presence of the tip does not influence the density distribution in the 2DEG, so that the electron bubble does not form and no contour lines appear. We confirmed this statement by studying the SCA images measured at different tip heights above the surface; away from nulling voltage, the images depend strongly on changing the tip height, whereas at nulling voltage they stay virtually unchanged.

In some cases, submicrometer structures similar to those discussed above persist at any voltage between the tip and the sample, including the nulling voltage for the Kelvin signal. By measuring the Kelvin signal as a function of the tip height, we have found that in such cases the tip does not have a uniform work function over its entire surface. Most probably, this results from GaAs debris partially covering the scanning tip. As a result, an electric field exists between the probe and the sample at any tip-sample voltage, even when the averaged Kelvin signal is 0. We therefore carefully checked the cleanliness of the tip throughout the experiments reported here. Possibly, in previous work (*3*), the tip-to-sample electric field was not completely eliminated and debris on the tip resulted in a nonuniform work function difference between different regions of the tip and the sample. Therefore, some of the features (particularly arcs and filaments) observed in figure 2 of (*3*) may be artifacts resulting from the tip locally perturbing the sample.

Imaging of another region of the sample at three different magnetic fields and tip-sample voltages is shown in Fig. 3. Each contour line marks a position within the 2DEG plane, where the number of electrons in the bubble changes by 1. As the tip voltage decreases, the energy of the N electron state drops relative to the N + 1 electron state, and the contour line moves. Monitoring the evolution of the images at a fixed field, we observe that contours shrink around the central locations as the voltage decreases toward nulling. We conclude that inside each contour the electron bubble has one more electron than outside. In particular, the contours surround two local minima of the potential (as sensed by electrons). Note that different contours follow the same evolution as we change the tip voltage to move one contour to a position formerly occupied by another. For example, at magnetic field $B = 6.5$ T, the inner contour at $+1.0$ V and the outer contour at $+0.5$ V appear indistinguishable in size and shape. This confirms our view of the bubble as an electrostatic potential probe; despite differences in bubbles created by different tip voltages, the resulting contours remain practically unchanged.

Our equipotential contours have the same meaning as topographic contours on a land map. To measure the amplitude of the electrostatic potential inside the 2DEG, we need to know the energetic separation between the single-electron contours. This information comes from measuring the width of the single-electron peaks in a SCA trace taken as a function of the tip voltage at a fixed location. We fit the shape of the single-electron peaks by the derivative of the Fermi distribution (*9*). Assuming that the width of the single-

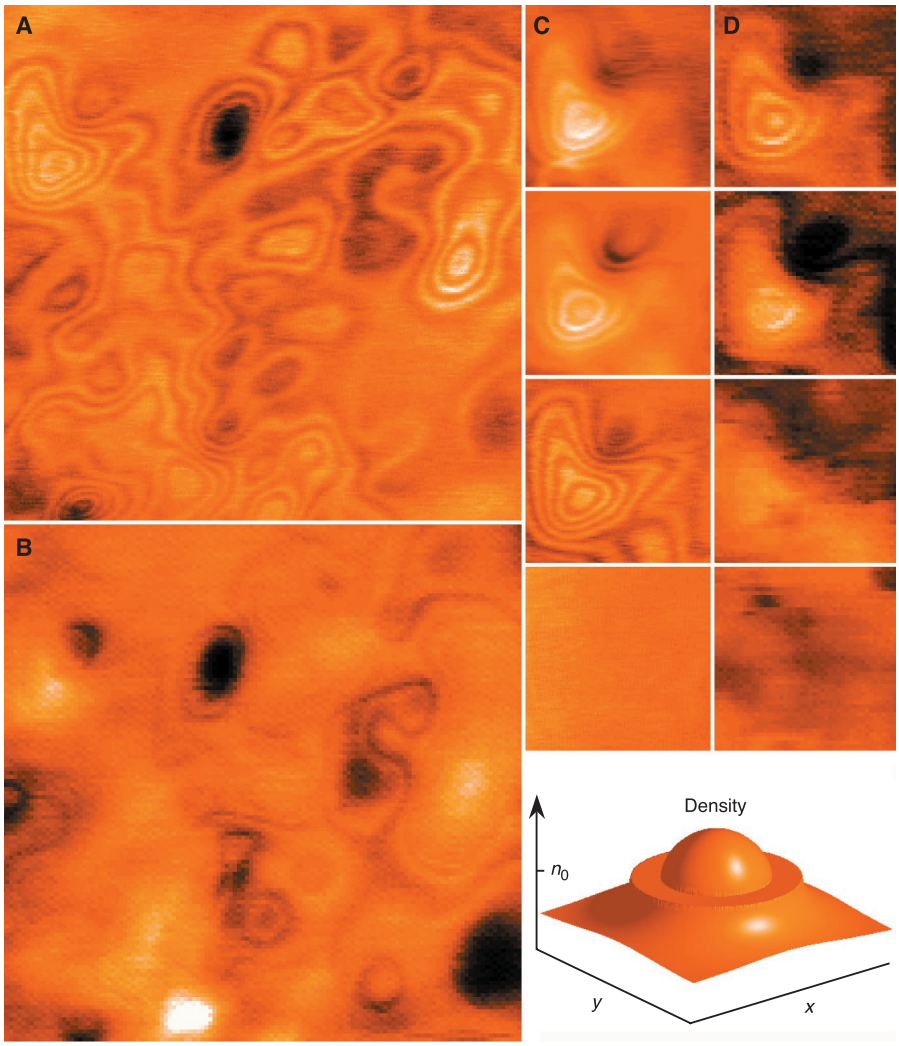

Fig. 2. (**A**) SCA image, 2.5 μm by 2.5 μm, at 5.8 T ($\nu \leq 1$) and $V_{tip} = +1$ V. (**B**) Image of the same region at 3.0 T ($\nu \leq 2$). (**C**) Magnetic field evolution of the feature at the top left corner of (A) at $V_{tip} = +1$ V. Top to bottom: 6.5, 6.1, 5.9, and 5.7 T. The features disappear when more than one spin-split Landau level is filled in the bulk ($\nu > 1$). (**D**) Evolution of the same feature with tip voltage, with $B = 6.0$ T. Top to bottom: 1.0, 0.7, 0.4, and 0.0 V. At the nulling voltage (lowest image), the tip does not influence 2DEG. Inset: schematic of the 2DEG density profile underneath the tip. Note the ring of constant density that corresponds to the incompressible strip with an integer Landau level–filling factor (inset).

electron peaks is determined by the temperature of 0.35 K, we find that the Fermi energy at the bubble is changed by ~2 meV per change of the tip voltage by 1 V. Also, as we change the tip voltage by 1 V, from +0.5 V to +1.5 V, at 6.6 T the innermost contour expands to span the entire area. We thus conclude that the range of the random potential in this region is about 2 meV.

The contour lines observed near bulk filling factor $\nu = 1$ reappear around $\nu = 2$ (compare Fig. 2, A and B). The contours observed at $\nu = 1$ display a stronger contrast, although the expected value of the exchange-enhanced spin gap ($\nu = 1$) is smaller than the cyclotron gap ($\nu = 2$). Tunneling of an electron between the interior and exterior of the bubble should be additionally suppressed close to $\nu = 1$ by the opposite spin orientation of the transferred electron in the initial and final states. This suppression of tunneling does not exist close to $\nu = 2$, and as a result the Coulomb blockade may be less pronounced in the latter case.

The contours clearly encircle the same locations at $\nu = 1$ and $\nu = 2$. The close similarity between the images indicates that we observe a fingerprint of the same random electrostatic potential at both filling factors. The random potential fluctuations extend laterally by typically ~0.5 to 1 μm. This scale appreciably exceeds 50 nm, the width of the spacer layer that separates 2DEG from donors. Random potential fluctuations due to remote ionized donors should have a characteristic lateral scale of approximately the spacer width (*14*). Most probably, screening by the residual electrons left in the donor layer smoothens the potential in our sample. Note that the size of the scanned bubble, ~100 nm (see below), in principle does not prevent observation of smaller scale potential fluctuations. Indeed, at select locations the single-electron contours display very small radii of curvature, signaling steep potential bumps or dips (Fig. 3).

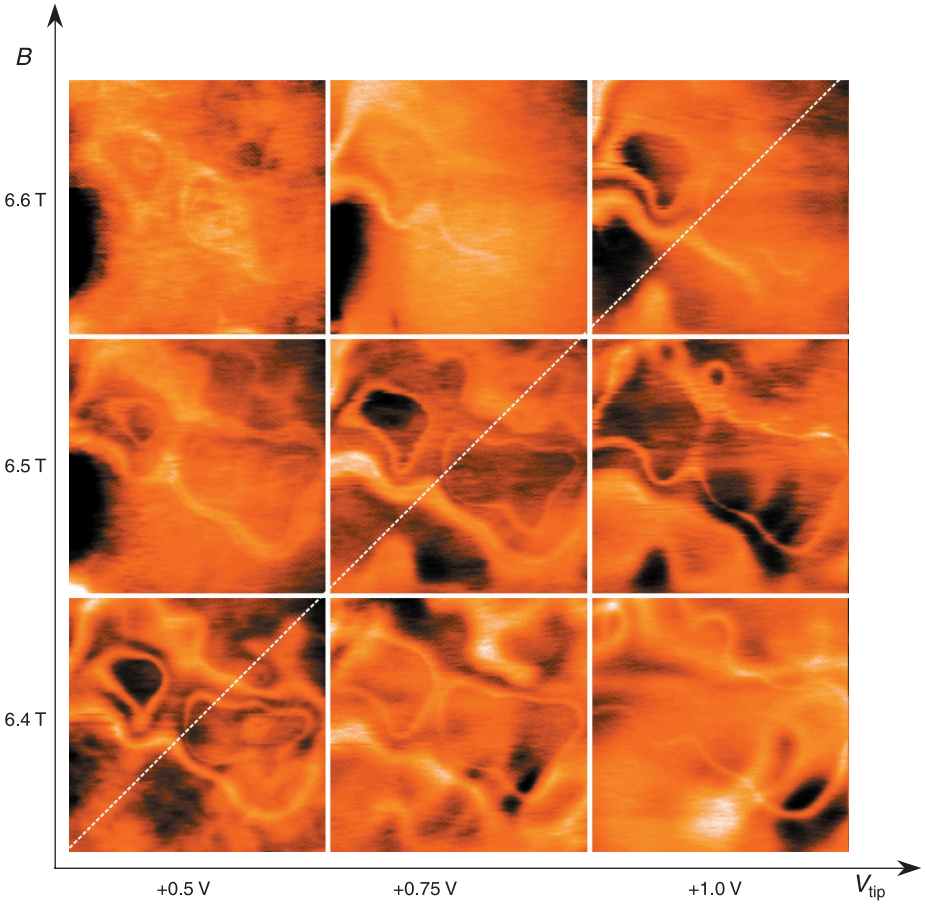

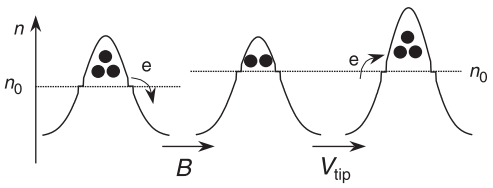

Fig. 3. Series of 2 μm by 2 μm SCA images taken at a different location from Fig. 2. The changes in contour size introduced by the tip voltage and magnetic field compensate each other. See images along the diagonal dashed line. Lower panel: Schematic explanation of the changes induced in the bubble by magnetic field and the tip voltage.

Figure 3 also traces the evolution of contours with magnetic field. Interestingly, the changes induced by variations of magnetic field and by the tip-sample voltage are quite similar. Indeed, we can compensate for the change of a contour's size induced by magnetic field by properly tuning the tip-sample voltage (Fig. 3, images along the dashed diagonal line). The size of contours remains constant at $\nu = 1$ along lines of $dV_{tip}/dB \approx 2V/T$. At $\nu = 2$, the constant shapes of contours are instead preserved at $dV_{tip}/dB \approx 4V/T$. We can readily explain this observation by recalling that the bubble is formed on top of an integer number of completely filled (spin-split) Landau levels. When magnetic field increases, the degeneracy of these levels grows, and they can accommodate more electrons. To supply these electrons, we need to apply a larger voltage between the tip and the sample. We expect the voltage required for compensation to be roughly proportional to the number of filled Landau levels, in agreement with the experiment.

We determine the size of the bubble by measuring the periodicity of the signal with magnetic field. Adding one flux quantum per area of the bubble adds one electronic state to each filled (spin-split) Landau level, removing roughly an electron from the upper, partially filled Landau level that constitutes the bubble. We observe that as the magnetic field is changed by ~0.2 T, the contours shift by one complete period. In Fig. 3, the inner contour at $B = 6.4$ T coincides with the outer contour at $B = 6.6$ T. For the case of Fig. 2, the magnetic field period has a similar value of ~0.15 T, implying an area of 0.02 μm^2. This compares favorably with the square of the 2DEG depth. Because the magnetic field period does not depend on location within the image, it appears that the size of the bubble is not strongly affected by the random potential.

In conclusion, we have formed a mobile quantum dot inside the 2DEG by locally accumulating electron density underneath the scanning probe. By comparing the Coulomb blockade patterns at different locations, we map the potential inside the 2DEG as sensed by the electrons. We find that the 2D electron screening of the random potential induced by external impurities changes little between different quantum Hall plateaus and within each plateau. With demonstrated single-electron sensitivity, our subsurface charge accumulation may enable understanding of a wide variety of submerged electronic structures on the nanometer scale.

References and Notes

1. R. E. Prange and S. M. Girvin, Eds., *The Quantum Hall Effect* (Springer-Verlag, ed. 2, 1990).
2. M. A. Eriksson *et al.*, *Appl. Phys. Lett.* **69**, 671 (1996).
3. S. H. Tessmer, P. I. Glicofridis, L. S. Levitov, R. C. Ashoori, M. R. Melloch, *Nature* **392**, 51 (1998).
4. K. L. McCormick *et al.*, *Phys. Rev. B* **59**, 4654 (1999).

5. A. Yacoby, H. F. Hess, T. A. Fulton, L. N. Pfeiffer, K. W. West, *Solid State Commun.* **111**, 1 (1999).
6. G. Finkelstein, P. I. Glicofridis, S. H. Tessmer, R. C. Ashoori, M. R. Melloch, *Phys. Rev. B* **61**, R16323 (2000).
7. A. L. Efros, *Solid State Commun.* **67**, 1019 (1988); A. M. Chang, *Solid State Commun.* **74**, 871 (1990); C. W. J. Beenakker, *Phys. Rev. Lett.* **64**, 216 (1990); D. B. Chklovskii, B. I. Shklovskii, L. I. Glazman, *Phys. Rev. B* **46**, 4025 (1992).
8. W. Shockley, H. J. Queisser, W. W. Hooper, *Phys. Rev. Lett.* **11**, 489 (1963).
9. L. P. Kouwenhoven *et al.*, in *Mesoscopic Electron Transport*, L. L. Sohn, L. P. Kouwenhoven, G. Schoen, Eds. (Kluwer Academic, Dordrecht, Netherlands, 1997), pp. 105–214.
10. R. C. Ashoori, *Nature* **379**, 413 (1996); R. C. Ashoori *et al.*, *Phys. Rev. Lett.* **68**, 3088 (1992); R. C. Ashoori *et al.*, *Phys. Rev. Lett.* **71**, 613 (1993).
11. Single-electron features may also be observed in the SCA imaging if there exist localized "puddles" of electrons formed within the quantum Hall liquid. In this case, a biased tip scanning across a puddle would act as a gate, changing the number of electrons in it. The SCA images would then exhibit concentric rings of high and low SCA signal. Because each puddle would have its own distinct series of electron additions, the set of rings from different puddles would superimpose. Experimentally, the bright and dark bands form a single network of contour lines that never intersect. Therefore, we conclude that there exists only one few-electron bubble formed under the tip.
12. N. C. van der Vaart *et al.*, *Phys. Rev. Lett.* **73**, 320 (1994).
13. Contour lines reappear when we apply negative tip-sample voltages depleting the 2DEG at $B < 6$ T, when more than one Landau level is filled in the bulk of the sample. Here, we attribute them to a Coulomb blockade in a bubble formed by quasi-holes in the filled Landau level. See also I. J. Maasilta and V. J. Goldman, *Phys. Rev. B* **57**, R4273 (1998); M. Kataoka *et al.*, *Phys. Rev. Lett.* **83**, 160 (1999).
14. A. L. Efros, *Solid State Commun.* **65**, 1281 (1988).
15. We thank L. S. Levitov and M. Brodsky for numerous discussions. Supported by the Office of Naval Research, the Packard Foundation, Joint Services Electronics Program, and the National Science Foundation Division of Materials Research.

16 March 2000; accepted 23 May 2000

Carbon Nanotube–Based Nonvolatile Random Access Memory for Molecular Computing

Thomas Rueckes,[1] Kyoungha Kim,[2] Ernesto Joselevich,[1] Greg Y. Tseng,[1] Chin-Li Cheung,[1] Charles M. Lieber[1,2]*

A concept for molecular electronics exploiting carbon nanotubes as both molecular device elements and molecular wires for reading and writing information was developed. Each device element is based on a suspended, crossed nanotube geometry that leads to bistable, electrostatically switchable ON/OFF states. The device elements are naturally addressable in large arrays by the carbon nanotube molecular wires making up the devices. These reversible, bistable device elements could be used to construct nonvolatile random access memory and logic function tables at an integration level approaching 10^{12} elements per square centimeter and an element operation frequency in excess of 100 gigahertz. The viability of this concept is demonstrated by detailed calculations and by the experimental realization of a reversible, bistable nanotube-based bit.

In the past several decades, there has been a nearly constant exponential growth in the capabilities of silicon-based microelectronics (*1*). However, it is unlikely that these advances will continue much into the new millennium, because fundamental physical limitations, which prevent current designs from functioning reliably at the nanometer scale, will be reached while at the same time exponentially rising fabrication costs will make it prohibitive to raise integration levels. Molecular electronics (*2, 3*) can in principle overcome these limitations of silicon technology, because it is possible to have single-molecule devices that are organized cheaply in parallel by self-assembly. Much effort in this area has been focused on organic molecules as device elements, with very recent demonstrations of irreversible switches (*4*) and large negative differential resistances (*5*) for ensembles of molecules sandwiched between metal electrodes. The connection of molecular switching elements to the molecular wires that will be required for high-density integration and the function of such structures remains a substantial challenge.

Nanometer-diameter single-walled carbon nanotubes (SWNTs) exhibit unique electronic, mechanical, and chemical properties that make them attractive building blocks for molecular electronics (*6, 7*). Depending on diameter and helicity, SWNTs behave as one-dimensional metals or as semiconductors (*8*), which, by virtue of their great mechanical toughness and chemical inertness, represent ideal materials for creating reliable, high-density input/output (I/O) wire arrays. However, viable strategies for introducing molecular-scale device functionality into such I/O lines have not been established. SWNTs have been used to make low-temperature single-electron (*9*) and room temperature field effect (*10*) transistors. Smaller devices based on intratube junctions have been proposed (*11*) and observed recently in experiments (*12*), although no approaches yet exist for either the controlled synthesis of nanotube junctions or the integration of many addressable junctions as needed for molecular-scale computing.

Our concept for integrated molecular electronics differs substantially from previous efforts (*2–5*), because it exploits a suspended SWNT crossbar array for both I/O and switchable, bistable device elements with well-defined OFF and ON states (Fig. 1). This crossbar consists of a set of parallel SWNTs or nanowires on a substrate and a set of perpendicular SWNTs that are suspended on a periodic array of supports (Fig. 1A). Each cross point in this structure corresponds to a device element with a SWNT suspended above a perpendicular nanoscale wire. Qualitatively, bistability can be envisioned as arising from the interplay of the elastic energy, which produces a potential energy minimum at finite separation (when the upper nanotube is freely suspended), and the attractive van der Waals (vdW) energy, which creates a second energy minimum when the suspended SWNT is deflected into contact with the lower nanotube. These two minima correspond to well-defined OFF and ON states, respectively; that is, the separated upper-to-lower nanotube junction resistance will be very high, whereas the contact junction resistance will be orders of magnitude lower. A device element could be switched between these well-defined OFF and ON states by transiently charging the nanotubes to produce attractive or repulsive electrostatic forces. On the basis of this switching mode, we can characterize the elements as nano- or molecular-scale electromechanical devices.

In the integrated system, electrical contacts are made only at one end of each of the lower and upper sets of nanoscale wires in the crossbar array, and thus, many device elements can be addressed from a limited number of contacts (Fig. 1B). At each cross point (n, m) in the array, the suspended (upper) SWNT can exist in either the separated OFF state or the ON state in contact with the perpendicular nanotube on the substrate (lower SWNT). The ON/OFF information at an (n, m) element thus can be read easily by measuring the resistance of the junction and, moreover, can be switched between OFF and ON states by applying voltage pulses

[1]Department of Chemistry and Chemical Biology, [2]Division of Engineering and Applied Sciences, Harvard University, Cambridge, MA 02138, USA.

*To whom correspondence should be addressed. E-mail: cml@cmliris.harvard.edu